AIAA JOURNAL
Vol. 40, No. 12, December 2002

Surface Topology on the Wheels of a Generic Four-Wheel Landing Gear

Barry Lazos*
NASA Langley Research Center, Hampton, Virginia 23681-2199

The analysis of shear stress lines in surface oil flow can provide attachment and separation characteristics on three-dimensional configurations about which flowfield data are often difficult or time consuming to acquire. This technique, in conjunction with mean surface pressure data, was utilized to determine the surface topology on a fore and aft wheel of a generic four-wheel landing gear model. Tests were performed at a Reynolds number of 6×10^5 based on wheel diameter. Because noise is produced when fluid attaches to or separates from a surface, the detailed analysis highlights regions on the wheels where further investigation may be warranted. The surface characteristics on the wheels determined in this study correlate well with the mean flowfield data acquired in a previous study. A relationship is hypothesized between observed changes in the state of separation on the ground side of the fore wheel in the present study, with the changing streamwise location of a midwheel vortex discovered in a previous study.

I. Introduction

EXPERIMENTAL measurement of three-dimensional flows is often difficult because the structure associated with them is often complex, which makes the flow difficult to probe. Even when this is not the case, measurement of even a single parameter throughout the entire three-dimensional space may be prohibitively time consuming. Therefore, the normal practice is to probe the flow in regions of suspected importance. Oftentimes, this procedure results in the omission of important details due to an inaccurate assessment of significant flow regions. One of the simplest and most effective ways to gather preliminary three-dimensional data and to determine important flowfield regions is through surface topology studies. Although Dallmann et al.[1] point out that features of the surface topology are not "sufficient to conjecture qualitative features within the outer (mid-air) flow field," locations of flow separation and attachment can be readily determined that highlight regions of important offsurface flow structure.

When an aircraft is in a high-lift configuration during landing approach, some geometrically complex structural features are exposed to the flow. One of the most complex is the landing gear, which is noted to be one of the dominant airframe noise sources on modern commercial aircraft.[2] Airframe noise results from pressure fluctuations created by interactions between the aircraft surface geometry and the surrounding fluid. The inherent bluff-body features of landing gear, as well as the complex arrangement of landing gear components, allow for noise production through the mechanisms of steady and unsteady wake flow, turbulent inflow, and vortex instability and deformation. A literature review by the author suggests that multiple wheel-set configurations are noisier than single wheel-set configurations. Heller and Dobrzynski[3,4] have suggested that this is due to an interaction of the wake from the fore wheels with the aft wheels. In a more recent study, Dobrzynski and Buchholz[5] suggest that such a tire-wake/tire interaction is not as significant noise a contributor as was previously suspected. Yet the authors still note that significant noise production occurs in the region between the inline wheels. This leads to speculation that developed flow structure may play a significant role in noise production for this configuration.

Although noise is a direct result of fluctuating flow features, insight into regions of noise production can be gained when considering only the mean flow features. In a previous work, Lazos[6] determined the mean velocity field around a generic four-wheel landing gear configuration with wheels and struts scaled to the main landing gear of a Boeing 757. The investigation utilized digital particle image velocimetry (DPIV) and tuft data to identify a nonstationary vortex that persists between the inline wheels on the ground side of the axle plane. That work, as well as the present, will be useful for validation of computational fluid dynamics (CFD) codes used for noise source determination.

In the current study, mean surface characteristics on the wheels of a four-wheel landing gear are studied. The model used is the same used by Lazos,[6] with tests conducted at the same Reynolds number based on wheel diameter of 6×10^5. Extraneous components of an actual four-wheel landing gear, such as brake mechanisms, tubing, and wheel hubs, were not included. Although such components are, admittedly, significant noise contributors, many of these can easily be eliminated or shielded by the manufacturer. The purpose of the present study is to highlight regions on a "clean" landing gear configuration that may warrant further investigation as potentially signficant noise sources and to provide experimental data for validation of computational codes. Data acquired include mean surface pressure and oil flow visualization on a fore and aft wheel. Surface topology characteristics are determined for each wheel utilizing both data sets. The following detailed analysis is intended to provide information that will aid in the determination of landing gear noise sources and advance the technique of surface topology assessment using oil flow visualization.

II. Experiments

A. Facility and Model

Experiments were conducted in the Basic Aerodynamics Research Tunnel (BART)[7] at NASA Langley Research Center. This facility is an open-circuit wind tunnel with a test section area of 71×102 cm and a length of 305 cm. The interior of the test section is visually accessible from all sides except the floor. The model used in the current study was a generic four-wheel landing gear configuration with wheels and supports scaled to 31% of those on a Boeing 757. Two of the wheels were produced from CIBA-Geigy 5180 resin using stereolithography. The other two were molded fiberglass. The cylindrical sections of the support structure were either steel or aluminum. Materials chosen for the model were a result of test and instrumentation requirements. One of the wheels was instrumented with 50 pressure ports along its spanwise periphery. It was made rotatable using a servomotor installed in the axle, which allow the

Received 16 July 2001; revision received 27 April 2002; accepted for publication 2 July 2002.

*Research Scientist, Department of Flow Physics and Control, Mail Stop 170.

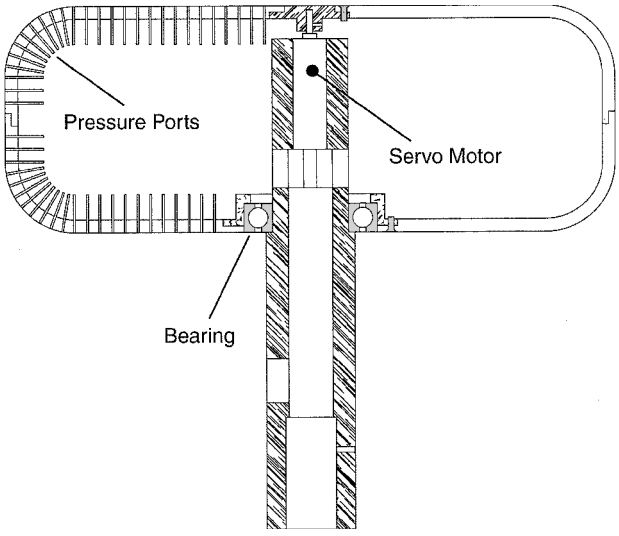

Fig. 1 Cutaway section of pressure ported wheel.

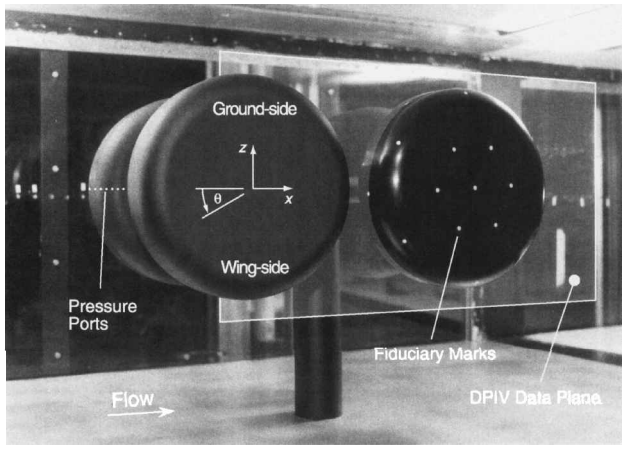

Fig. 2 Model installed in BART facility.

ports to be accurately positioned at any azimuthal angle around the wheel. Figure 1 shows a cut-away sketch of the ported wheel with the motor and pressure ports highlighted. Another of the wheels was marked at precise locations with fiduciary points to aid in oil flow visualization data analysis. This wheel was attached to the axle with a setscrew so that it could be easily removed and photographed after each test run.

B. Data Acquisition and Analysis

Tests performed for the current study included measurements of mean surface static pressures and oil flow visualizations on a fore and aft wheel. Figure 2 is an image of the model installed upside down in the tunnel test section. Highlighted in Fig. 2 are the pressure taps along the periphery of one of the wheels and the fiduciary points on another. Also highlighted in Fig. 2 is the DPIV plane in which the velocity field around the wheels was resolved, the results of which are reported by Lazos.[6]

Mean static pressures were acquired on the ported wheel surface using an electronically scanned pressure acquisition system. The transducer range was chosen such that most of the available scale was utilized without exceeding the range limits. Pressures were acquired around the entire wheel circumference at measurement stations every 2 deg by rotating the wheel via the servomotor. Positioning accuracy using the servomotor was determined to be approximately ± 0.3 deg. At each measurement station, 30,000 data samples were acquired simultaneously at each of the 50 ports over a 90-s period. The samples acquired at each port were then averaged to produce the mean. Surface static pressures were measured on both a fore and an aft wheel by simply rotating the model 180 deg around the center support strut to position the ported wheel in the front or rear. The pressure transducers were accurate within ± 1.379 N/m^2 if their temperature was maintained within $\pm 1^\circ$C. Therefore, the pressure acquisition system was recalibrated whenever the ambient temperature in the test area, where the transducers were located, varied beyond this range.

Oil flow visualizations were conducted to highlight the shear stress lines on the wheels. A test run began by first applying a 50/50 mixture of kerosene and titanium dioxide powder to a wheel with the tunnel flow off. Immediately after application of the mixture, the test section was closed, and the tunnel was rapidly brought up to speed. A constant speed was then maintained until the oil mixture was sufficiently dry. Both fore and aft wheel data were acquired on the wheel marked with fiduciary points (Fig. 2) by placing it either in the front or in the rear of the model.

Eight images were acquired of the wheel using a digital camera with an image resolution of 3060×2036 pixels. An image of the outboard side of the wheel was first acquired with the wheel in place in the test section. The oil on this surface was then removed. Then, with the aid of a large suction cup, the wheel was removed from the test section and placed in a photographic booth without disturbing the remaining oil film. Here, an additional seven images were acquired: one of the inboard side of the wheel and six around the wheel periphery (tread area), one every 60 deg. After the images were collected, each was mapped onto a three-dimensional computer representation of the experimental model. The fiduciary points on the wheel were used for accurate placement of each image.

The extension of the experimental data into virtual space provided for an effective means of data visualization to perform a topological analysis of the shear stress lines represented in the oil. Methods used to carry out the analysis were those of Kaplin,[8] Lighthill,[9] Perry and Fairlie,[10] Tobak and Peake,[11] and Chapman and Yates.[12] These methods utilize critical point concepts of nonlinear differential equations to identify patterns in the shear stress vector field that occur at points where skin friction is zero. In addition, the current analysis uses the concepts of Maskell[13] to identify three-dimensional separation along a line that gives rise to a free vortex layer. Joint mapping of the pressure data with the oil flow data aided the analysis, especially in the identification of regions of flow attachment.

Patterns in the shear stress lines expected in the current study are shown in Fig. 3 along with associated terminology and color coding used in the following discussion. Patterns on the left represent flow attachment, whereas patterns on the right represent flow separation. The topological phenomenon associated with flow attachment or separation along a line is referred to as a bipartition. The line itself is termed a bipartite line and can occur in association with a saddle point or in isolation. When a bipartite line is associated with a saddle point, the separation/attachment is termed closed and will be identified in the following discussion as a solid line. When a bipartite line is in isolation, the separation/attachment is termed open and will be identified as a dashed line. The terms open and closed are taken from the work of Wang.[14] To further delineate flow features, a bipartite line is termed positive if surface shear stress lines diverge from it (flow attachment) and negative if surface shear stress lines converge on it (flow separation). The terms positive and negative are taken from the work of Hornung and Perry.[15] Coloring of bipartite lines in the following discussion will be lavender to indicate flow attachment and fuchsia to indicate separation.

The composite images presented in this report reveal oil flow and surface pressure signatures on the fore and aft wheels. Mean surface static pressure is represented as a dimensionless pressure coefficient, $C_p = (P - P_s)/(P_t - P_s)$, where P is the measured pressure, P_s is the tunnel static pressure, and P_t is the tunnel total pressure. Color-coding of the pressure identifies the highest pressure in white and the lowest in blue. Renderings of the shear stress lines are in yellow or blue, whichever color best contrasts with the background pressure coloring. Arrows are included to indicate perceived flow direction.

While performing the following analysis, specifics of the surface flow topology in certain regions could not readily be discerned due to insufficient resolution of the oil flow technique and/or low surface shear stresses. Therefore, it must be emphasized that, in these regions, the flow attachment and separation features highlighted may not portray actual flow conditions. The possibility that the suspected

flow conditions exist, however, was ensured by using the method of indexing as described by Yates and Fearn.[16]

III. Experimental Results and Discussion

A. Fore Wheel

Figure 4 is an image of the outboard side of the fore wheel after an oil flow visualization run. Typical fiduciary points are highlighted. Surface static pressure is represented by color gradation and renderings of the perceived shear stress lines are in yellow with arrows to indicate direction. The orientation of the data maintains the wind-tunnel convention such that the ground side of the wheel is at the top and the wing side is at the bottom. The flow direction is indicated as left to right.

At the front of the wheel in Fig. 4, a significant favorable pressure gradient is evidenced by the rapid color change in the pressure signature from red to deep blue and is associated with the acceleration of fluid around the outboard edge. The flow here is expected to be laminar, and at the end of surface curvature, separation is initiated at the saddle of separation A due to a sudden adverse pressure gradient. Just downstream, the flow is expected to transition, resulting in reattachment at the saddle B. Saddles A and B form negative- and positive-closed bipartitions, respectively, that extend along the forward edge of the wheel. Between them the surface flow direction is predominantly toward the saddles, which results in a pooling of oil at the forward edge of the wheel. Following the negative bipartite lines beginning at A, the flow direction along them becomes increasingly aligned with the freestream direction as the wing and ground sides of the wheel are approached. Along the positive bipartite lines beginning at B, however, the flow direction becomes increasingly opposed to the freestream direction as the wing and ground sides of the wheel are approached. Eventually, the flow along these lines is unable to maintain this opposition to the freestream and nodes of attachment form at points C, where the flow direction reverses to follow positive-open bipartite lines. Note, too, that the direction of the surface flow between the bipartite lines also changes and is now directed away from the saddles, toward the edges of the wheel.

Downstream of the positive-closed bipartition formed by B in Fig. 4, the flow along the outboard face of the wheel is expected to be turbulent. At the downstream edge of the wheel, surface curvature results in another adverse pressure gradient, and turbulent separation occurs. Separation here is seen to be a complex combination of saddles, nodes, and bipartitions, some of which will be discussed later in a different view of the wheel. On the ground side of the wheel, surface shear stress lines merge at D to form a negative-open bipartition. On the wing side of the wheel, a small pool of oil forms behind a saddle of separation at E. One end of the bipartite line through E terminates in the focus F, whereas the other end terminates at the node G. In the middle of the wheel, another saddle of separation forms at H, with the bipartite line through it terminating at nodes G and I. Just downstream of H, another saddle of separation is shown at J. Between H and J, a region of increased pressure is apparent. Close analysis of the shear stress lines in this region reveals the probability of a node of attachment at K.

Figure 5 is an image of the inboard side of the fore wheel. At the forward edge, the flow is similar to that on the outboard side of the wheel. An adverse pressure gradient results in flow separation beginning at saddle A. The flow is expected to then transition and reattach to the surface at saddle B. Between the closed bipartitions formed by these saddles, oil again pools as the surface flow there is directed predominantly toward the saddles. The bipartite lines through A proceed around the edge of the wheel with flow along them directed toward the wing and ground sides of the wheel. The bipartite lines through B terminate, and the nodes labeled C are formed along with positive-open bipartitions.

Just downstream of saddle B in Fig. 5, the presence of the wheel axle results in a severe adverse pressure gradient. Just ahead of the axle a saddle of separation and a node of attachment are highlighted and labeled D and E, respectively. Between this saddle/node combination, the flow is expected to recirculate in the juncture of the wheel and axle. It is hypothesized that the juncture flow here is turbulent because the surface flow ahead is expected to be turbulent. Further evidence to support this hypothesis is found in the experimental work of Pierce and Tree,[17] where turbulent juncture flow was studied using smoke and surface oil flow visualization as well as laser Doppler velocimetry. In their study, the authors documented the existence of a single horseshoe vortex that was strongly time variant with large changes in size and position. They also noted that the time-averaged center of the vortex "appeared to coincide with a clear, well scoured line around the [cylinder] in the surface flow visualization." Such a line is highlighted in Fig. 5. Similar results are presented by Pierce and Harsh[18] using surface oil flow visualization and Eckerle and Langston[19] using five-hole probe measurements in conjunction with surface oil flow visualization.

Immediately downstream of the axle (Fig. 5), a clearly distinguishable negative-open bipartition begins at F and ends in a focus of separation at G. In the wake region of the axle on the wing side, surface streamlines rapidly turn and wrap into the focus. On the ground side, surface streamlines make a much broader arc, extending nearly to the downstream edge of the wheel before turning back upstream toward the axle. These opposed flow directions result in a saddle of separation at H. Surface fluid in the wing side of the wake that does not turn back upstream leaves the surface of the wheels at the saddle of separation I.

Differences in the surface flow characteristics on the wing- and ground-side edges of the wheel outside the axle wake are postulated to result from the presence of the center support strut. On the wing-side face of the wheel, a rapid acceleration around the edge of the wheel is suggested by the highly favorable pressure gradient in that region. This is seen as the rapid color gradation from yellow, to green, to blue. It is expected that the flow here is locally accelerated as it passes between the wheel and center support strut. A sudden adverse pressure gradient then results in the formation of a small separation bubble beginning at the saddle of separation J and ending at the node of attachment K. On the ground side of the wheel, the pressure gradient is not as favorable, and surface shear stress lines converge to form a negative-open bipartition beginning at L.

Figure 6 shows negative and positive bipartite lines, seen earlier in Figs. 4 and 5. They are labeled B and C, respectively, and extend up over the edges of the wheel to the ground-side face, possibly influencing flow separation characteristics there. In the center of Fig. 6, there are two adjacent pools of oil labeled 1 and 2, aligned in the streamwise direction. Both of these pools are expected to highlight distinct zones of recirculating fluid under a complex paring of separation bubbles that merge and divide with time. Zone 1 begins with the saddle-of-separation labeled A at about −92 deg around the wheel from its leading edge. It is bounded on either side by the bipartite lines formed by A, and terminates at the intersection of these bipartite lines with the bipartite lines B. Zone 2 begins immediately downstream and appears to form as the negative and positive bipartite lines B and C tend toward the center of the wheel and the fluid between them merges from the left and the right.

During testing, the topological features associated with recirculation zones 1 and 2 were observed to change erratically between two states. Changes were particularly apparent at the downstream end of recirculation zone 2. For much of the time, zone 2 appeared to be distinctly bounded, with the internal oil tightly contained. At times, however, the trailing edge of this boundary appeared to burst, which resulted in the expulsion downstream of some of the internally contained fluid. This state change in topological features is expected to result from a time-dependent structural bifurcation of the flow pattern as described by Chapman and Yates.[12] Though an exact description of the surface flow details is not possible due to low spatial resolution of the oil flow technique, speculation of the structural changes is presented in Fig. 7.

Figure 7a shows the anticipated structural features of the primary flow state. Here a saddle-of-attachment D and its associated bipartition make up the trailing edge of recirculation zone 2. The bounding sides of this zone are speculated to be negative-open bipartitions that form as the shear stress lines converge and the surface flow separates. The upstream boundary is a positive-open bipartition E that terminates along with other shear stress lines at a node of separation F. Figure 7b shows the anticipated structural features of the secondary flow state. In this case, the node of separation F becomes a focus of separation and the positive bipartition

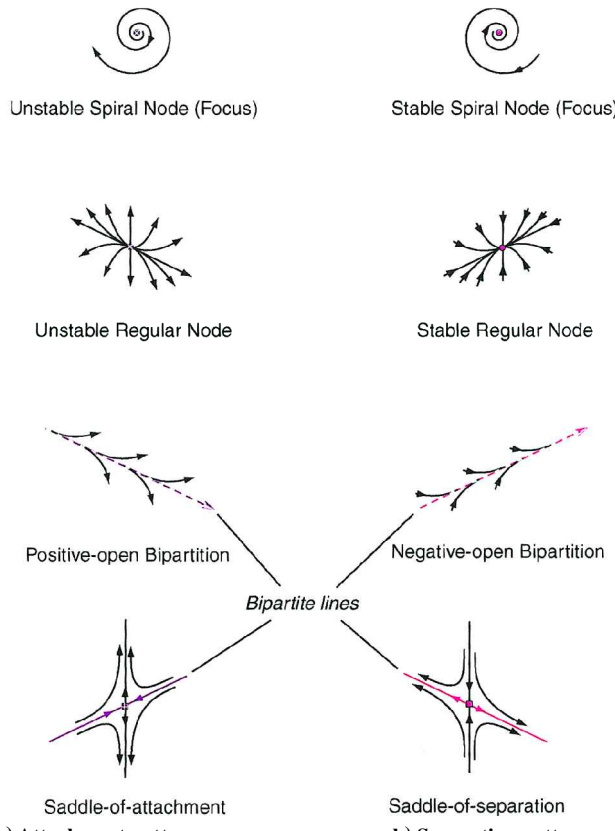

a) Attachment patterns **b) Separation patterns**

Fig. 3 Surface topology patterns at locations of flow separation and attachment expected in the current study.

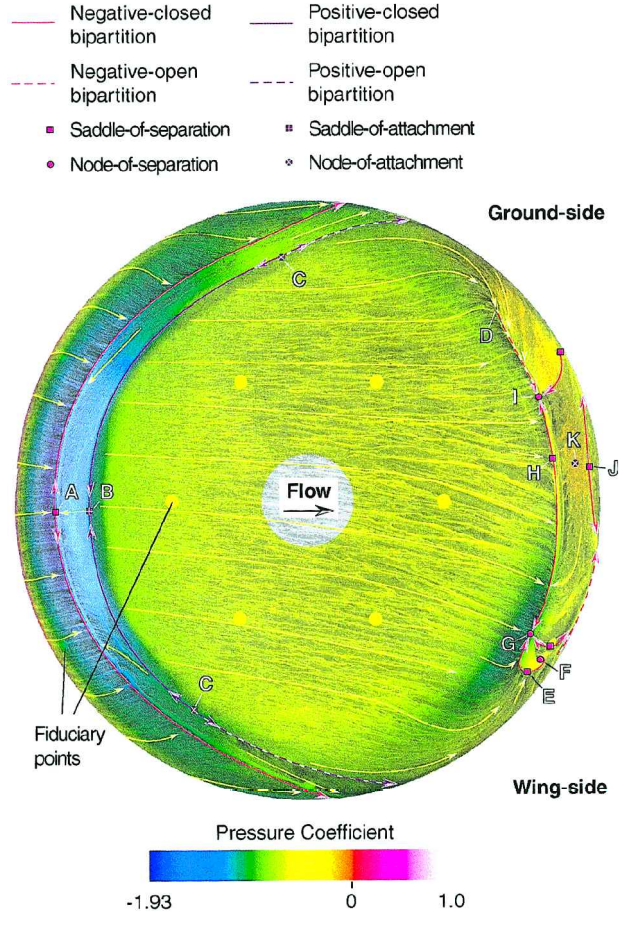

Fig. 4 Outboard side of the fore wheel showing surface static pressure and oil flow data, as well as perceived shear stress lines and locations of flow attachment and separation.

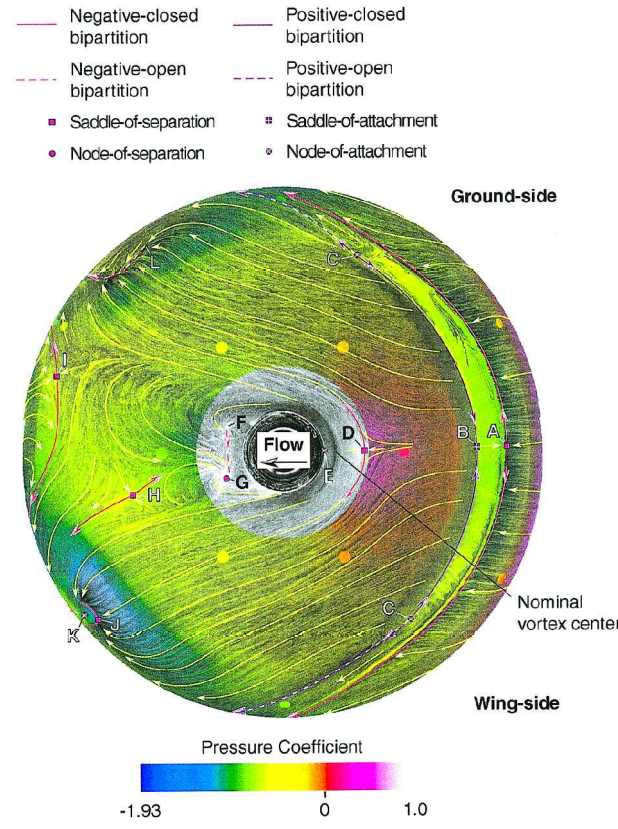

Fig. 5 Inboard side of the fore wheel showing surface static pressure and oil flow data, as well as perceived shear stress lines and locations of flow attachment and separation.

E in Fig. 7a is eliminated, opening the boundary between zones 1 and 2. Downstream, the saddle of attachment becomes a node of attachment D as the positive-open bipartite lines C are redirected downstream, and the bounding sides of zone 2 become saddles of separation G.

On the wing-side face of the wheel, shown in Fig. 8, some flow features look similar to those on the ground-side face, but here only a single pool of oil is seen. On this side of the wheel, the negative and positive bipartite lines, B and C, extend over the edges of the wheel and tend toward the center of the wheel as before. Flow separation, however, is initiated at about 97 deg around the wheel from its leading edge at saddle A. This is about 5 deg beyond that on the ground-side face. This results in a relative position difference, from the ground-side face, between the negative bipartite lines B and the trailing edge of the recirculation zone behind A. As a result, the formation of a second recirculation zone downstream, as was seen on the ground-side face, may be inhibited.

Here, on the wing-side face of the wheel, the inboard bipartite line beginning at A rolls up into a focus of separation at D. These separation characteristics are similar to what Hornung and Perry[15] refer to as a Werlé–Legendre separation. This type of separation is shown in Fig. 9, with Fig. 9a representing the two-dimensional pattern in the shear stress lines and Fig. 9b a perspective view of the inferred offsurface flow characteristics. As in the present experimental case, separation is initiated at a saddle of separation through which a bipartition is formed. One end of the bipartition rolls up into a focus, while the other continues downstream. Also shown in Fig. 9 is a positive-open bipartition, where shear layer attachment is induced by the separating vortical rollup. In Fig. 8, such a bipartition is not apparent in the surface pattern until much farther downstream at E. Because of its lateral and downstream position, however, it is unlikely that the bipartition E is associated with the upstream separation features.

Flow features on the back face of the fore wheel are extremely complex, as shown in Fig. 10. Whereas it might be expected that shear stresses here be relatively low, making it difficult to distinguish surface topology, in most regions the opposite is true. Surface

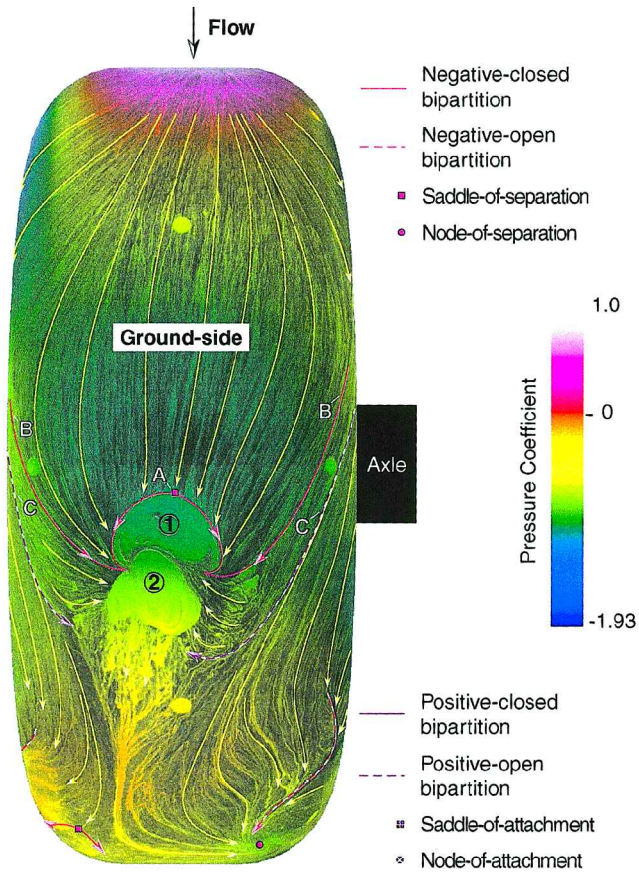

Fig. 6 Ground-side face of the fore wheel showing surface static pressure and oil flow data, as well as perceived shear stress lines and locations of flow attachment and separation; numbered regions identify perceived flow recirculation zones.

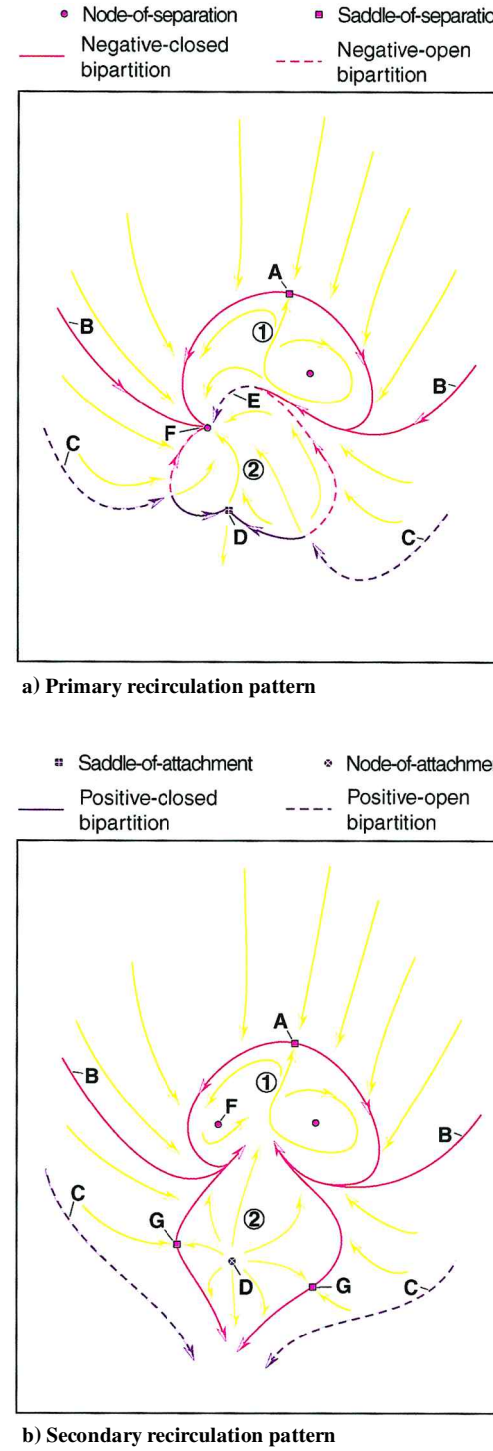

a) Primary recirculation pattern

b) Secondary recirculation pattern

Fig. 7 Hypothesized states of recirculation associated with separation on the ground-side face of the fore wheel.

flow direction and shear stress patterns are easily discernible in all locations except the outboard edge of the wheel, where flow features had to be more judiciously determined. In this region, shear stresses are low, which makes it sometimes difficult to ascertain surface topology. Here, the method of indexing was particularly useful, limiting the possibilities of suspected topologies.

The boundaries of this separated region are suspected to consist of six different negative bipartitions, one open and five closed, each terminating in either a node or focus of separation. On the ground side, the bounding edge consists of a negative bipartition beginning at the saddle A. This bipartition terminates on one side at the node B and on the other at the focus C. The upstream and downstream boundaries are also initiated at saddles of separation D and E, respectively. (These were mentioned earlier for Fig. 4 and labeled H and J, respectively.) The bipartition through D terminates at the nodes B and F, and the bipartition through E terminates at foci C and G. Note again the node of attachment H, which was mentioned earlier for Fig. 4 and labeled K, whose presence is suspected by the pressure and shear stress features there and is corroborated through the method of indexing.

In Fig. 10, the wing-side boundary of the separated region on the outboard edge of the wheel is suspected to be complex, consisting of two negative-closed bipartitions and a negative-open bipartition. One of the closed bipartitions begins with saddle I and ends at the node F and the focus J. It is readily identifiable by the pool of oil that forms behind it. The open bipartition begins at K in Fig. 10 and ends at the focus G. The other closed bipartition begins at the saddle of separation L. Though not immediately apparent in the shear stress lines, this saddle is expected from application of the method of indexing.

A closer look at the surface topology reveals why a saddle must be located in the vicinity of L. Consider two sources of attached fluid. One is a point source at the node of attachment H, at the center of the wheel. The other is a regional source where attached fluid is rounding the wing side of the wheel at M. Fluid that attaches to the surface at H that is not entrained in the focus G or the node F must continue toward the wing side of the wheel. Attached fluid from the wing side of the wheel at M, entering through the gap between J and K must either exit the surface to the right along the open bipartition, to the left at the focus J or the node F, or continue along the surface toward the ground side of the wheel. Surface fluid from the sources M and H not exiting the surface must at some point meet and form a stagnation point (singularity), most likely in the form of a saddle of separation like L.

At the wing side of the wheel (Fig. 10), a small pool of oil forms behind a saddle of separation N, where a small separation bubble is initiated. Directly downstream is the associated node of attachment O. Issuing from this region on either side of O are thick lines of oil

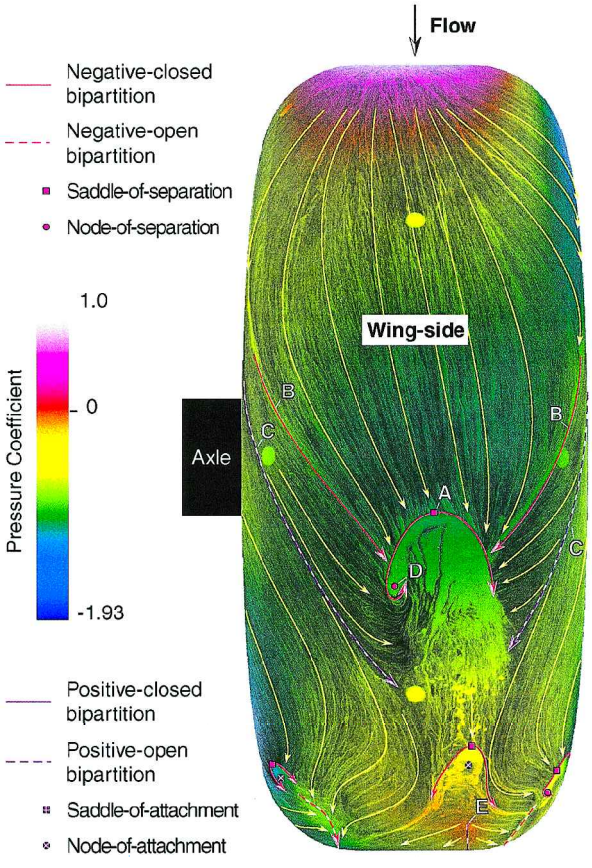

Fig. 8 Wing-side face of the fore wheel showing surface static pressure and oil flow data, as well as perceived shear stress lines and locations of flow attachment and separation.

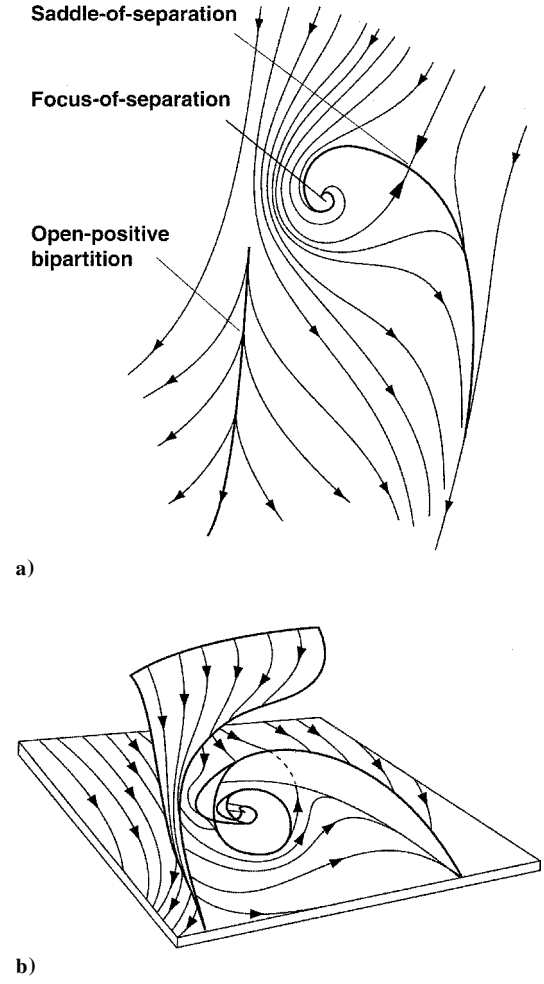

Fig. 9 Surface and offsurface characteristics of Werlé–Legendre separation (taken from Fig. 16 of Ref. 13).

identifying the path of the bipartition formed by N. On the outboard side, this bipartition joins with the negative-open bipartition at K, and on the inboard side, terminates at the focus P. As was seen earlier in Fig. 5, high-speed fluid from the inboard side of the wheel separates and reattaches to form a small bubble denoted by the saddle of separation at Q and the node of attachment at R in Fig. 10. Immediately downstream of this bubble, a negative-open bipartition S forms, terminating at the focus P. At the ground-side end of the wheel, attached fluid separates along the open bipartition T that terminates at the focus U.

At the center of the wheel image in Fig. 10, two flow attachment features are rendered. One is a node of attachment at V, and the other is an open bipartition at W. This bipartition was seen earlier in Fig. 8 and was mentioned in association with a Werlé–Legendre separation. Both the node and the bipartition are responsible for the saddle of separation at X that results as fluid issuing from each approaches a central point and stagnates. Node V is also important in the formation of saddle E, which was already mentioned, and the saddles Y and Z.

B. Aft Wheel

Mean surface flow features on the front face of the aft wheel are shown in Fig. 11. Here two large regions of flow attachment are highlighted and are made apparent by the extreme high surface static pressure and the lack of shear stress lines in the oil flow. From these regions, attached fluid issues in all directions along the wheel surface. Fluid approaching the center of the wheel from both the wing and ground sides stagnates, and two separate saddles-of-separation are formed at A and B. The bipartitions associated with them extend separately over the inboard side of the wheel, but on the outboard side they merge, and flow separation terminates. Between these two saddles a high-pressure region and stagnated flow suggest a node of attachment. The possibility of this combination of topological features is confirmed using the method of indexing, and the node is labeled C in Fig. 11.

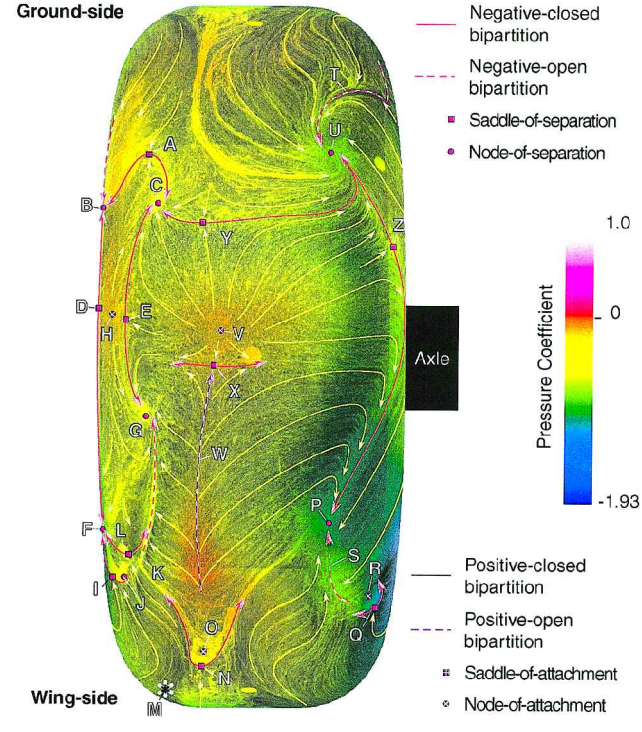

Fig. 10 Rearward face of the fore wheel showing surface static pressure and oil flow data, as well as perceived shear stress lines and locations of flow attachment and separation.

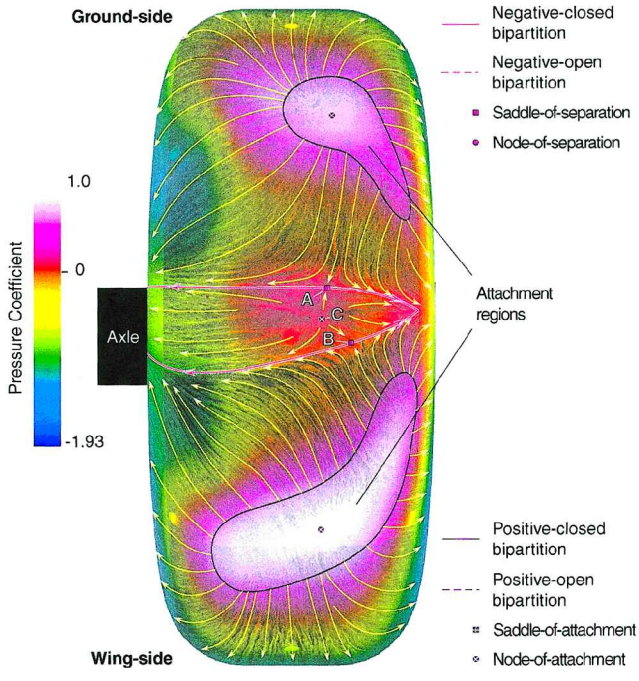

Fig. 11 Forward face of the aft wheel showing surface static pressure and oil flow data, as well as perceived shear stress lines and locations of flow attachment and separation.

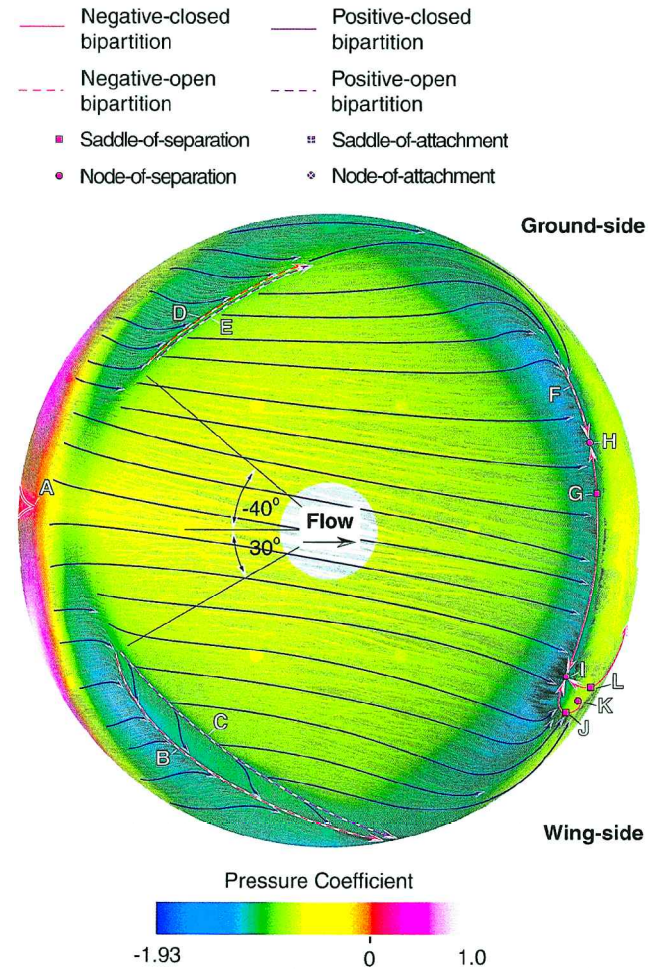

Fig. 12 Outboard side of the aft wheel showing surface static pressure and oil flow data, as well as perceived shear stress lines and locations of flow attachment and separation.

In Figs. 12 and 13, shear stress lines are rendered in blue to better contrast with the background pressure color. Figure 12 is an image of the outboard side of the aft wheel. The label A at the front of the wheel highlights the location where the bipartitions created on the forward face of the wheel merge. Downstream of this point, the shear stress lines indicate that the flow remains attached all of the way to the trailing edge of the wheel. This is expected to be due to the high-pressure apparent near A that eliminates the severe adverse pressure gradient necessary for separation to begin.

Separation features in the shear stress lines can not be seen on the forward edge of the aft wheel until about −40 deg on the ground side and 30 deg on the wing side, as noted in Fig. 12. On the wing side of the wheel, shear stress lines at the front edge are seen to diverge suddenly from their original path to follow a common line, labeled B in Fig. 12, where flow is expected to separate along a negative-open bipartition. Just downstream of this line is a region of slow moving surface fluid, apparent by the lack of well-defined shear stress lines in the oil film. Following this, shear stress lines are again readily apparent and directed downstream. This flow topology suggests flow attachment along the line labeled C, which is expected to be a positive-open bipartition. Both the positive and negative bipartite lines, B and C, extend over the wing-side edge of the wheel, where they merge and terminate. On the ground side of the wheel, separation characteristics are similar to the wing-side. However, on this side, a region of low-speed surface flow following the negative-open bipartition D cannot be detected before the shear stress lines straighten in the downstream direction. This suggests that flow reattaches immediately downstream of separation along a positive-open bipartition, labeled E.

At the downstream edge of the aft wheel in Fig. 12, separation characteristics appear similar to those seen at the downstream edge of the fore wheel in Fig. 4. On the wing side, shear stress lines converge to separate along a negative-open bipartition labeled F. Toward the center of the wheel, a saddle of separation forms at G with the bipartition through it terminating at the nodes H and I. At the lower boundary of the separated region, a small pool of oil forms, in front of which another saddle of separation is expected, labeled J. One end of the bipartition through J terminates at the node I, whereas the other end terminates at the focus K. Though not clearly apparent in the oil flow, the method of indexing suggests the formation of another saddle of separation in the vicinity of L. One end of the bipartition through this saddle terminates at the node I, whereas the other terminates at a focus (not seen in Fig. 12), on the rearward face of the wheel.

Figure 13 is an image of the inboard side of the aft wheel. Comparison between Figs. 13 and 5 shows that significant differences exist between the pressure signatures on the inboard sides of the aft and fore wheels. On the aft wheel, an extreme adverse pressure gradient is not apparent in front of the axle, as was the case on the fore wheel. Such a difference is likely due to differences in the flowfields that each wheel encounters. As opposed to the fore wheel, severe distortion is expected in both the mean and turbulent flowfields surrounding the aft wheel. Such distortions may tend to reduce pressure concentrations.

Separation characteristics also differ significantly between the aft and fore wheels. Shear stress lines along the wheel edge near A on the aft wheel are directed toward the axle and do not highlight a region of flow separation. Along B, however, shear stress lines rounding the edge of the wheel suggest flow separation beginning at C along a negative-open bipartition with immediate reattachment along the positive-open bipartition D. Between A and B, negative-closed bipartitions created on the front face of the wheel extend over the edge. As they extend downstream, they are skewed toward the wing side of the axle, where they merge and terminate.

Around the axle (Fig. 13), a vortex dominates the juncture flow beginning at the saddle of separation E. The shear stress lines associated with the vortex suggest it is highly skewed toward the wing-side of the wheel, which results in an offset node of attachment at F. The bipartition associated with saddle E is apparent around the entire axle with both ends extending downstream to the edge of the wheel, where they merge and terminate. Wake features in the shear stress lines behind the axle on the aft wheel are less apparent than those on the fore wheel. This can be expected because randomness in

the magnitude and direction of the edge velocities of turbulent eddies entrained in the rear axle wake will tend to eliminate mean macrostructure of the same scale.

Images of the wing- and ground-side faces, as well as the rearward face of the aft wheel, are not presented because the shear stress and pressure features on these faces were either trivial or could not be interpreted. Local flow acceleration over the wing- and ground-side faces of the aft wheel is apparent in the pressure signature, but singularities in the shear stress lines are not evident. This indicates the flow does not separate at saddles to form recirculation zone, as was the case on the fore wheel. On the ground-side face, flow separation is not suspected till about −120 deg around the wheel from the leading edge. Here, negative-open bipartitions appear likely to form, but the surface mean flow velocity is so low that distinct topological features are not readily apparent. On the wing-side face, flow separation is obvious along a negative-open bipartition as shear stress lines converge along the streamwise centerline of the wheel, at about 110 deg around the wheel from the leading edge. On the back face of the aft wheel, the near surface flow is expected to be dominated by a random wake containing entrained turbulent eddies that produce random velocity fluctuations. This randomness results in low mean shear stresses on the rearward face of the wheel, making it difficult to identify characteristics of the flow topology. In fact, the mean momentum was so low here that during testing the flow of oil over the surface seemed at times to be dominated by gravitational forces rather than shear forces.

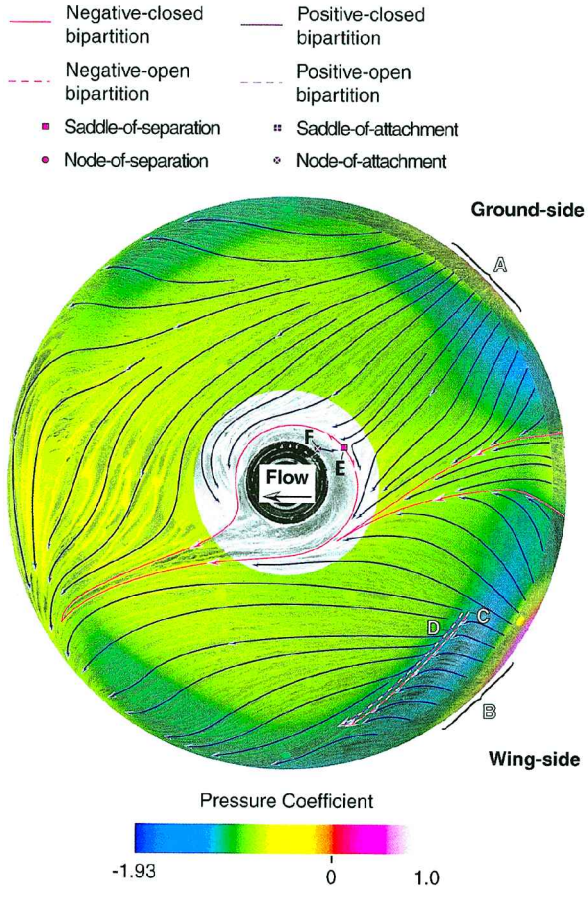

Fig. 13 Inboard side of the aft wheel showing surface static pressure and oil flow data, as well as perceived shear stress lines and locations of flow attachment and separation.

C. On- and Offsurface Flow Comparison

In a previous study,[6] mean velocity measurements were made in a vertical plane bisecting the inline wheels using DPIV. The model used in that study was the same one used in the current study. The results of the previous study revealed a nonstationary vortical rollup between the inline wheels that persisted on the ground side of a plane through the axles. It was speculated, from tuft visualizations, that the streamwise position of the vortex between the wheels was dependent on the separation characteristics on the back of the fore wheel. The following discussion will attempt to correlate the results of the previous study with those of the present study. Note that, in the end view images of the wheels presented in the current study, the laser light sheet bisecting the inline wheels in the previous study was aligned with the centers of the fiduciary points located at the spanwise centers of the wheels.

Figure 14 is an image of the mean velocity field around the inline wheels presented as Fig. 5 in Ref. 6. Streamline features are readily apparent and velocity magnitude is represented with color. Locations of flow attachment and separation are highlighted, as well as specific streamlines between the wheels. Note, first, that in Fig. 14 a region of flow attachment is highlighted on the back of the fore wheel. This corresponds well with the shear stress and pressure signatures on the back face of the fore wheel in Fig. 10, where an increase in pressure corresponds to a rendered positive-open bipartition W. Both the pressure and shear stress signatures suggest flow attachment.

The vortical rollup seen behind the fore wheel in Fig. 14 is also suggested by the shear stress signature in Fig. 10. Fluid separating from the front of the aft wheel travels upstream to impact the back of the fore wheel resulting in the node V. The saddle Y in Fig. 10 is the separation location highlighted in Fig. 14, where fluid leaves the back surface of the fore wheel to roll up into a vortex. Both the saddle Y in Fig. 10 and the separation location in Fig. 14 are at −160 deg around the wheel from its leading edge and coincide directly with

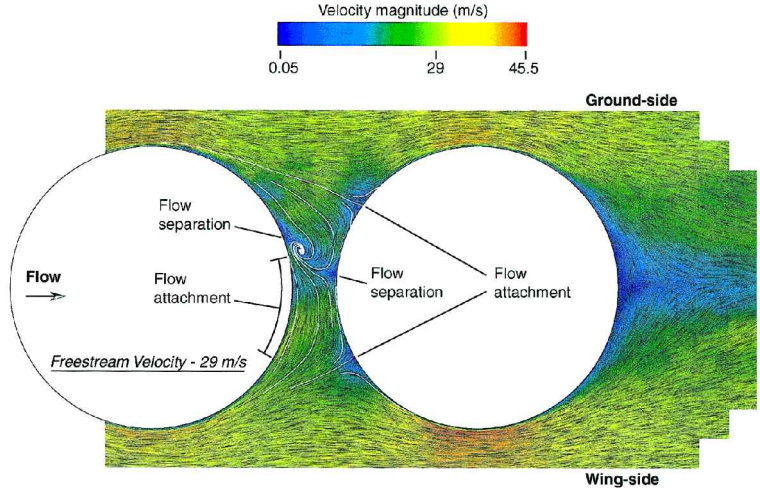

Fig. 14 Velocity magnitude and direction in DPIV plane bisecting inline wheels; streamlines between wheels highlighted in white (taken from Fig. 5 of Ref. 6).

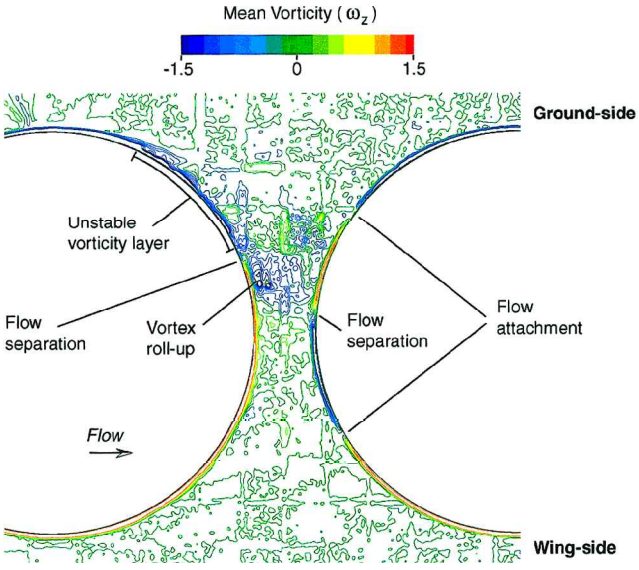

Fig. 15 Mean vorticity field in midplane of wheels (taken from Fig. 9 of Ref. 6).

the separation location observed using tuft visualization by Lazos.[6] The fact that the saddle-of-separation X and the separation bubble, denoted by saddle N and node O in Fig. 10, are not apparent in Fig. 14, is expected. As already mentioned, the plane of the laser light sheet used to acquire the velocity data passes through the fiduciary points along the vertical midplane of the wheels and is, therefore, offset to the inboard side of these singularities.

Referring again to the velocity data of Fig. 14, attachment and separation locations on the front of the aft wheel are also apparent in the pressure and shear stress signatures. The locations of the two attachment regions on the front face of the aft wheel in Fig. 11 correspond extremely well with their locations determined from Fig. 14. The saddles of separation, A and B, in Fig. 11 are depicted in Fig. 14 as the separated flow region on the front of the aft wheel. The node of attachment C is not apparent in the velocity data, which is likely due to the resolution of the DPIV data and the offset of the data plane to the inboard side of the singularity.

When Fig. 6 was discussed, it was mentioned that observations on the ground-side face of the fore wheel during testing suggested topological features there alter between two different states, one state more temporally dominant than the other. The expected topological features of each state were presented in Fig. 7. Lazos[6] noted that separation features on the back of the fore wheel near the ground side change state. Again, one state was more temporally dominant than the other. It was also suggested by Lazos[6] that this change in separation features on the fore wheel altered the streamwise position of the midwheel vortex. If the topological changes on the ground side of the fore wheel are directly related to the changing separation characteristics on the back of the fore wheel, then they are ultimately responsible for the change in streamwise position of the midwheel vortex.

It is hypothesized that when topological features on the ground side of the fore wheel are as shown in Fig. 7a, the flow downstream of recirculation zone 2 is attached up to −160 deg around the wheel, and the midwheel vortex rests against the back of the fore wheel. However, when the topological features of Fig. 7b are realized, the flow downstream is massively separated and the midwheel vortex is repositioned downstream to rest against the front of the aft wheel. Added support for this hypothesis is given in Fig. 15, taken from Lazos,[6] showing an unstable vorticity layer on the back of the fore wheel beginning at about −113 deg. This azimuthal location directly corresponds with the downstream end of recirculation zone 2 seen in Fig. 6.

IV. Conclusions

The current study examined the mean surface static pressure and topological features on a fore and aft wheel of a generic four-wheel landing gear, scaled to 31% of a Boeing 757 main landing gear. The purpose of the study was to identify regions around the wheels that warrant further investigation as potentially significant noise sources and to provide detailed mean flow information for validation of CFD codes. The carfully detailed analysis of the shear stress features on the wheels is intended, as well, to advance the technique of surface topology assessment using oil flow visualization. Tests were conducted at a Reynolds number based on wheel diameter of 6×10^5. Mean surface pressures were acquired over most of the wheel surface using 50 pressure taps distributed along the spanwise periphery of the wheel. The wheel could be rotated 360 deg so that the pressure taps could be located at any azimuthal angle. Mean surface topology was determined by applying a suspension of kerosene and titanium dioxide powder to the wheel surface and running the facility at the test speed until the oil mixture was sufficiently dry. Analysis of the surface topology was performed in detail in an effort to advance the technique of topological feature assessment using oil flow visualization.

The results highlight regions of flow separation and attachment on the fore and aft wheels. Many should be investigated further as potentially significant regions of noise production. In particular, separation on the outboard trailing edges of the fore and aft wheels occurs over a broad area incorporating several singularities and bipartitions of various types. On the inboard sides of the wheels, turbulent juncture vortices form where the wheels and axles connect. The back faces of the aft wheels are noted to be massively separated with surface characteristics typifying small scales and random velocity fluctuation.

The most complex combination of surface flow features was found on the back face of the fore wheel. On this portion of the model, shear stresses were remarkably high in most places such that separation and attachment topologies could be readily identified. On the front face of the aft wheel, two large attachment regions are apparent on the wing and ground sides. Surface flow converging toward the center of the wheel from these attachment region is noted to separate along bipartitions created by two saddles of separation. In a previous report,[6] velocity field data in the vertical midplane identified a nonstationary vortical rollup that persists between the inline wheels. In the current study, mean surface flow features on both the front face of the aft wheel and the back face of the fore wheel correlated extremely well with the results of the previous velocity data. Changing topological features on the ground-side face of the fore wheel are hypothesized to be responsible for the changing separation characteristics on the back of the fore wheel and, ultimately, the erratic streamwise position of the mid-wheel vortex.

It is hoped that the data presented and analyzed in such great detail will be useful for validation of computational codes and for the advancement of surface topology assessment using oil flow visualization. Note that the idealized clean four-wheel configuration used resembles an actual landing gear in only its most basic form and that the data presented herein are likely to provide only a general understanding of possible flow features on an actual four-wheel configuration. It is suspected, however, that the region between the inline wheels of an actual four-wheel landing gear will prove to be a region of significant noise generation, as suggested in this study.

References

[1] Dallmann, U., Hilgenstock, A., Riedelbauch, S., Schulte-Werning, B., and Vollmers, H., "On the Footprints of Three-Dimensional Separated Vortex Flows Around Blunt Bodies," *Vortex Flow Aerodynamics, Symposium of the Fluid Dynamics Panel in Scheveningen, The Netherlands*, CP-494, AGARD, 1990, pp. 9-1–9-13.

[2] Michel, U., Barsikow, B., Helbig, J., Hellmig, M., and Schüttpelz, M., "Flyover Noise Measurements on Landing Aircraft with a Microphone Array," AIAA Paper 98-2336, June 1998.

[3] Heller, H. H., and Dobrzynski, W. M., "Sound Radiation from Aircraft Wheel-Well/Landing Gear Configurations," *Journal of Aircraft*, Vol. 14, No. 8, 1977, pp. 768–774.

[4] Heller, H. H., and Dobrzynski, W. M., "Unsteady Surface Pressure Characteristics on Aircraft Components and Farfield Radiated Airframe Noise," AIAA Paper 77-1295, Oct. 1977.

[5] Dobrzynski, W. M., and Buchholz, H., "Full-Scale Noise Testing on Airbus Landing Gears in the German Dutch Wind Tunnel," *Proceedings of*

the 3rd AIAA/CEAS Aeroacoustics Conference (18th AIAA Aeroacoustics Conference), AIAA, Reston, VA, 1997, pp. 98–111.

[6]Lazos, B. S., "Mean Flow Features Around the Inline Wheels of Four-Wheel Landing Gear," *AIAA Journal*, Vol. 40, No. 2, 2002, pp. 193–198.

[7]Sellers, W. L., and Kjelgaard, S. O., "The Basic Aerodynamics Research Tunnel—A Facility Dedicated to Code Validation," AIAA Paper 88-1997, 1988.

[8]Kaplin, W., *Ordinary Differential Equations*, Addison Wesley Longman, Reading, MA, 1958, pp. 415–470.

[9]Lighthill, M. J., "Boundary Layers and Separation," *Laminar Boundary Layers*, edited by L. Rosenhead, Clarendon, Wotton-Under-Edge, England, U.K., 1963, pp. 72–82.

[10]Perry, A. E., and Fairlie, B. D., "Critical Points in Flow Patterns," *Turbulent Diffusion in Environmental Pollution*, edited by F. N. Frenkiel and R. E. Munn, Vol. 18B, Academic Press, New York, 1974, pp. 299–315.

[11]Tobak, M., and Peake, D. J., "Topology of Three-Dimensional Separated Flows," *Annual Review of Fluid Mechanics*, 1982, Vol. 14, pp. 61–85.

[12]Chapman, G. T., and Yates, L. A., "Topology of Flow Separation on Three-Dimensional Bodies," *Applied Mechanics Review*, Vol. 44, No. 7, 1991, pp. 329–345.

[13]Maskell, E. C., "Flow Separation in Three Dimensions," Royal Aircraft Establishment, Rept. RAE-AERO-2565, Farnborough, England, U.K., 1955.

[14]Wang, K. C., "Boundary Layer Over a Blunt Body at High Incidence with an Open-Type of Separation," *Proceedings of the Royal Society of London, Series A: Mathematical and Physical Sciences*, Vol. 340, No. 1620, 1974, pp. 33–55.

[15]Hornung, H., and Perry, A. E., "Some Aspects of Three-Dimensional Separation, Part I: Streamsurface Bifurcations," *Zeitschrift Für Flugwissenschaften Und Weltraumforschung*, Vol. 8, No. 2, 1984, pp. 77–87.

[16]Yates, L. A., and Fearn, R. L., "The Determination of the Topological Structure of Skin Friction Lines on a Rectangular Wing-Body Combination," NASA CR-4168, 1988.

[17]Pierce, F. J., and Tree, I. K., "The Mean Flow Structure on the Symmetry Plane of a Turbulent Junction Vortex," *Journal of Fluids Engineering*, Vol. 112, March 1990, pp. 16–22.

[18]Pierce, F. J., and Harsh, M. D., "Three-Dimensional Turbulent Boundary Layer Separation at the Junction of a Streamlined Cylinder with a Flat Plate," *Flow Visualization III*, Hemisphere, New York, 1985, pp. 331–335.

[19]Eckerle, W. A., and Langston, L. S., "Horseshoe Vortex Formation Around a Cylinder," *Journal of Turbomachinery*, Vol. 109, 1987, pp. 278–285.

P. J. Morris
Associate Editor

Color reproductions courtesy of NASA Langley Research Center.